Supplementary Information:

Morphological Insights into Se-Driven Charge Transport and Enhanced Performance in $Sb_2(S,Se)_3$ Solar Cells

Yeeun Lee[1]†, Hongjae Shim[2]†, Mingrui He[2]†, Kaiwen Sun[2], Mohammad Moein Seyfouri[1,3], Lei Wang[1], Jan Seidel[1], Chen Qian[2]*, Xiaojing Hao[2]*, Jae Sung Yun[2,4]*

[1]School of Materials Science and Engineering, University of New South Wales, Sydney, NSW 2052, Australia

[2]Australian Centre for Advanced Photovoltaics (ACAP), School of Photovoltaic and Renewable Energy Engineering, University of New South Wales, Sydney, NSW 2052, Australia

[3]X-ray facilities, Mark Wainwright Analytical Center, University of New South Wales, Sydney, NSW 2052, Australia

[4]School of Computer Science and Electronic Engineering, Advanced Technology Institute (ATI), University of Surrey, Guildford, Surrey GU2 7XH, United Kingdom

*Corresponding authors: c.qian@unsw.edu.au, xj.hao@unsw.edu.au, j.yun@surrey.ac.uk

†These authors contributed equally to this work.

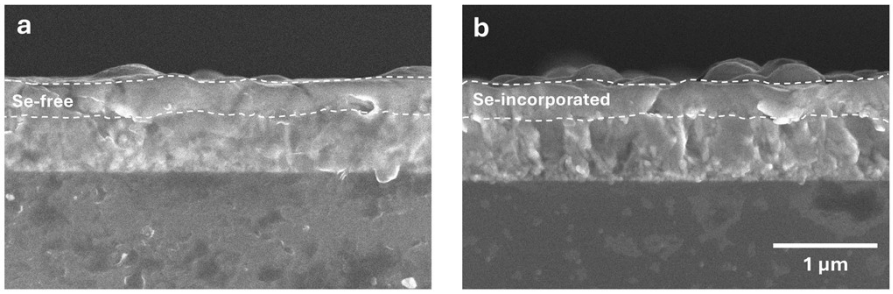

Figure S1. Cross-sectional scanning electron microscopy (SEM) images of (a) the Se-free, and (b) the Se-incorporated final films

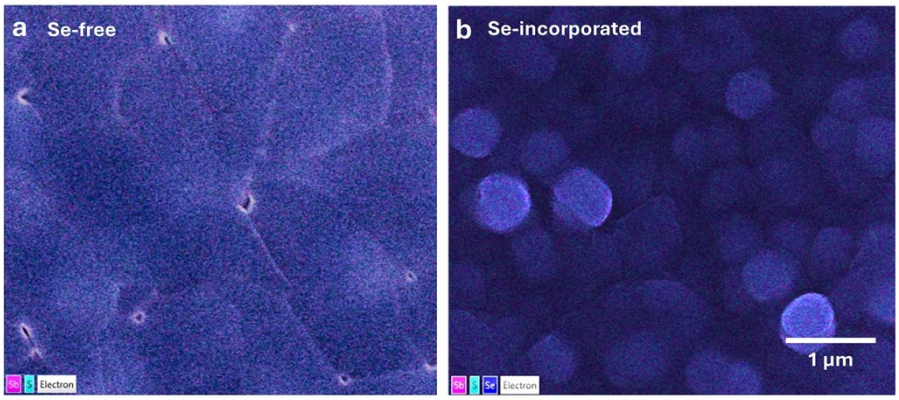

Figure S2. Energy-dispersive spectroscopy (EDS) surface scans of (a) the Se-free, and (b) the Se-incorporated final films

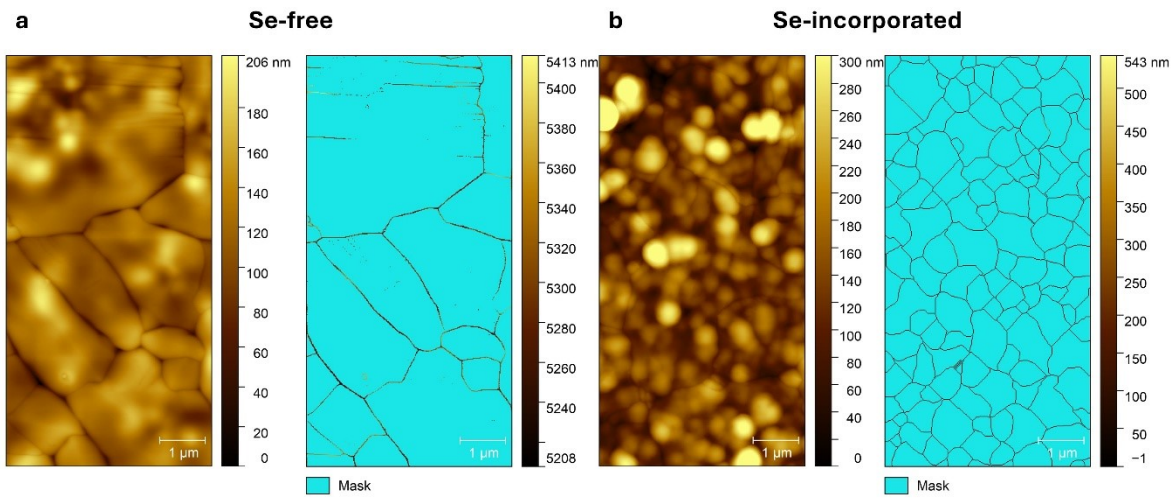

Figure S3. Large-area atomic force microscopy (AFM) topography scans and corresponding grain boundary (GB) masks for (a) Se-free and (b) Se-incorporated films. Each image set shows the topography (left) and the GB mask (right) derived from the same scan area, highlighting differences in grain size and GB density.

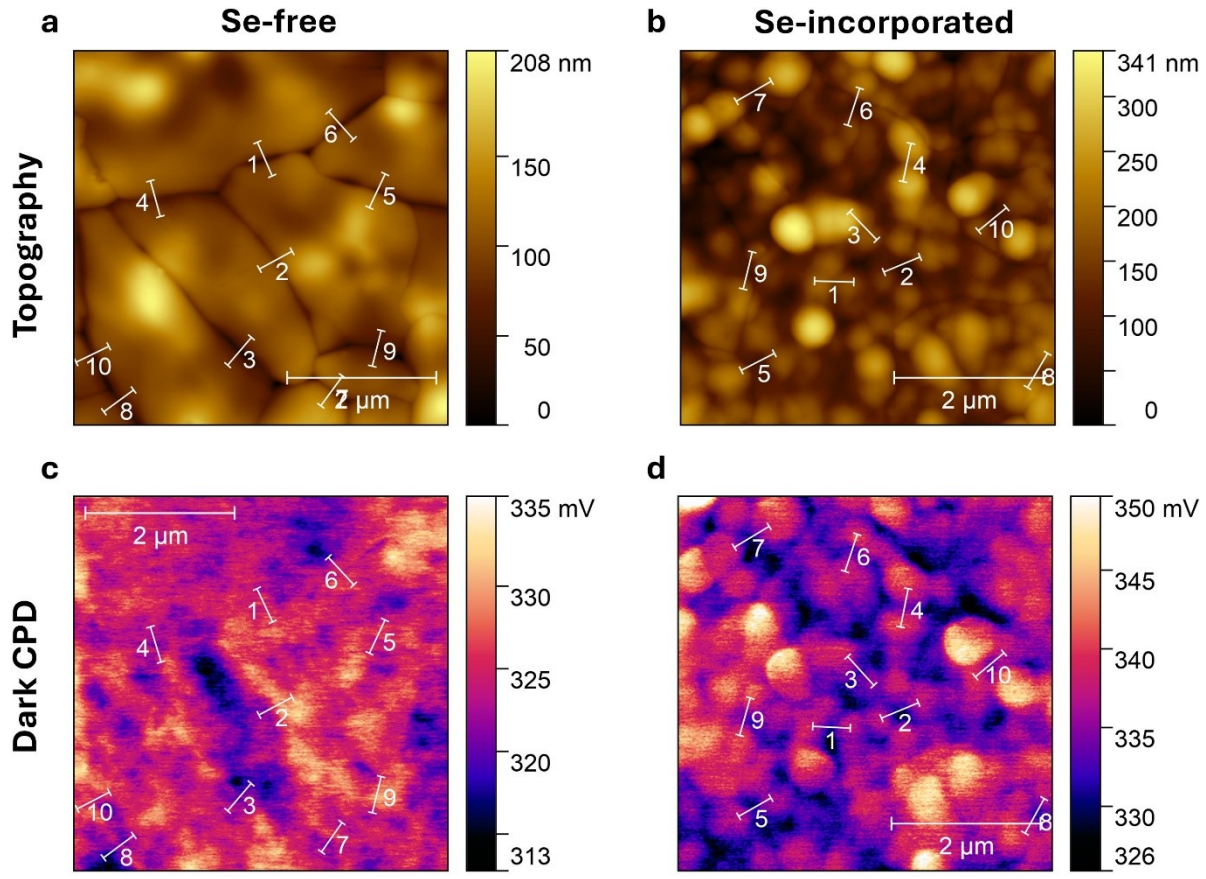

Figure S4. Locations of ten representative line profiles marked on (a, b) the AFM topography images and corresponding (c, d) contact potential difference (CPD) images under dark conditions for Se-free and Se-incorporated films, respectively.

Table S1. Measured GB slopes, corresponding angles relative to the x-axis, and dihedral angles (φ) for Se-free and Se-incorporated samples, obtained from linear fits of AFM topographic profiles across selected GBs.

Sample	Left Slope	Angle (°) w.r.t. x-axis (Left)	Right Slope	Angle (°) w.r.t. x-axis (Right)	Dihedral Angle φ (°)
Se-free	-0.519	-27.420	0.468	25.069	127.511
	-0.393	-21.443	0.302	16.820	141.737
	-0.444	-23.926	0.334	18.464	137.609
	-0.508	-26.946	0.332	18.390	134.664
	-0.530	-27.932	0.601	30.997	121.071
	-0.812	-39.092	0.307	17.081	123.827
	-0.355	-19.566	0.205	11.610	148.824
	-0.474	-25.351	0.580	30.101	124.548
	-0.285	-15.896	0.345	19.024	145.079
	-0.767	-37.480	0.803	38.780	103.740
				Average	**130.861**
Se-incorporated	-0.364	-20.004	0.103	5.893	154.103
	-0.444	-23.928	0.170	9.673	146.399
	-0.405	-22.064	0.299	16.637	141.299
	-0.238	-13.384	0.303	16.851	149.765
	-0.364	-19.993	0.274	15.306	144.701
	-0.109	-6.218	0.151	8.571	165.211
	-0.427	-23.105	0.448	24.125	132.770
	-0.496	-26.368	-0.048	-2.730	156.363
	-0.259	-14.504	0.113	6.439	159.057
	-0.278	-15.521	0.127	7.263	157.217
				Average	**150.688**

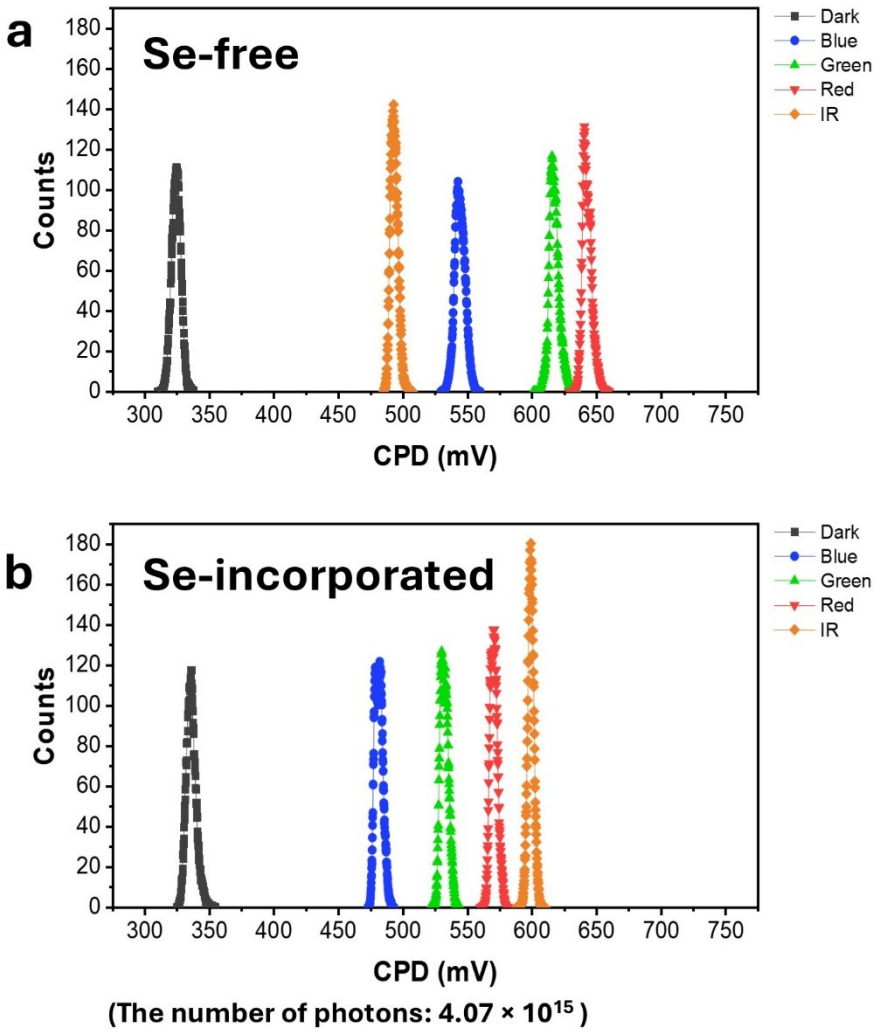

Figure S5. Histograms of CPD distributions under dark conditions and various illuminated conditions for (a) Se-free and (b) Se-incorporated films.

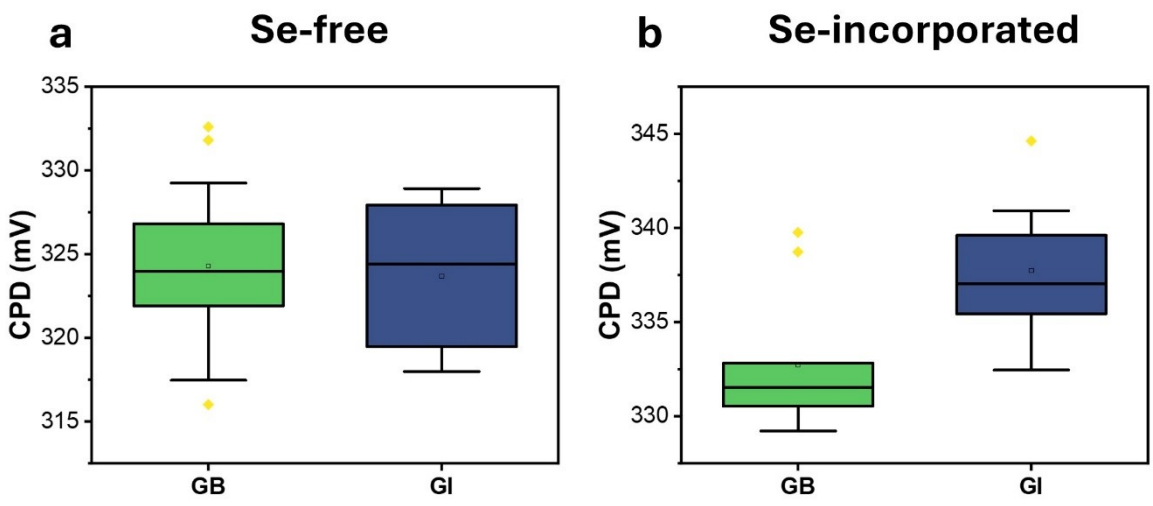

Figure S6. Box plots of CPD values measured at GBs and GIs for (a) Se-free and (b) Se-incorporated films under dark conditions.

Table S2. Mean CPD values and corresponding full width at half maximum (FWHM) under dark and various illuminated conditions for Se-free and Se-incorporated films.

Sample	Se-free		Se-incorporated	
	CPD (mV)	CPD FWHM (mV)	CPD (mV)	CPD FWHM (mV)
Dark	324.33	8.5	335.54	8.23
Blue	544.03	9.48	481.09	8.01
Green	616.76	7.93	531.86	7.85
Red	642.18	7.85	570.3	6.95
IR	493.07	6.89	599.11	5.34
Average	524.07	8.13	503.58	7.28

Supplemental Note:

To evaluate lateral potential uniformity under different illumination conditions, CPD histograms were extracted from dark and light-exposed KPFM CPD maps for both Se-free and Se-incorporated films (**Figure S5**). Illumination was provided using monochromatic light sources at 406nm (blue), 532nm (green), 635nm (red), and 808nm (infrared), each with a photon flux of 4.7×10^{15} photons. The CPD distributions were fitted with Gaussian functions to extract the mean CPD values and FWHM, summarized in **Table S2**.

The Se-incorporated film consistently exhibits narrower FWHM values across all illumination conditions. This indicates that the Se-incorporated film is a more laterally uniform surface potential compared to the Se-free film. Additionally, the higher CPD of 599.11 mV observed in the Se-incorporated film under infrared (IR) illumination, compared to 493.07 mV for the Se-free film, can be attributed to enhanced IR absorption resulting from Se incorporation. The Se-incorporated film has a narrower bandgap due to Se incorporation, enabling more efficient absorption of IR light and generating a greater number of photocarriers.

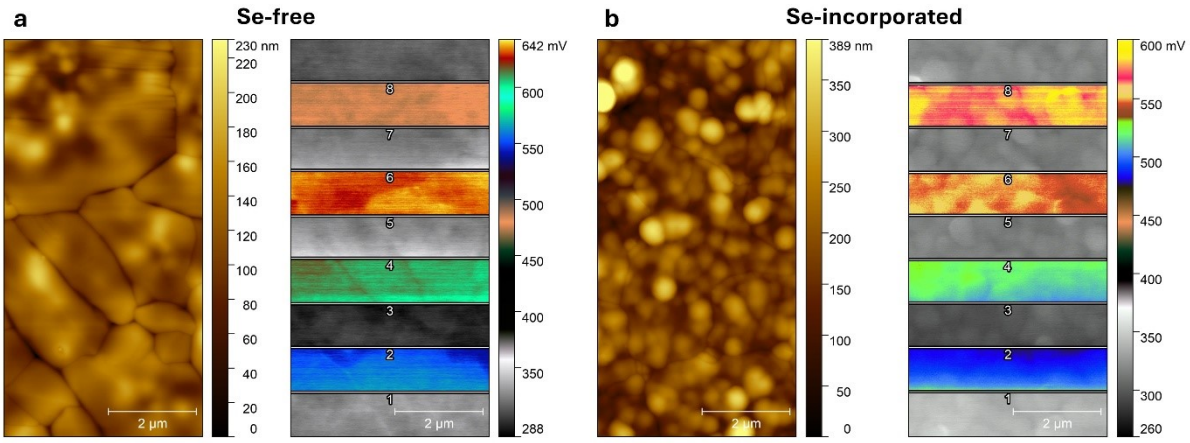

Figure S7. AFM topography map and timed-resolved Kelvin probe force microscopy (tr-KPFM) maps of (a) Se-free and (b) Se-incorporated films deposited on Glass/FTO/CdS substrates under dark and illuminated conditions.

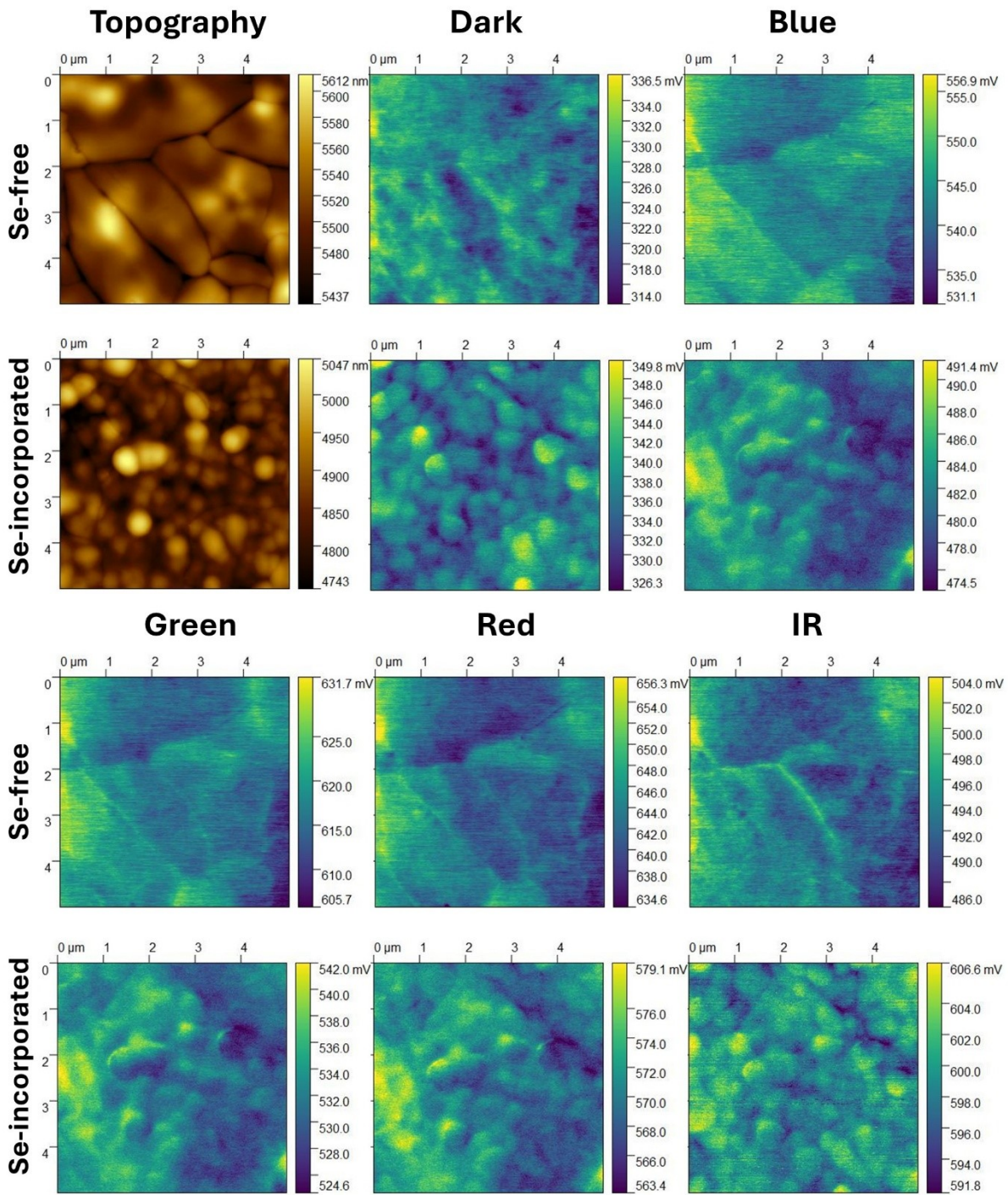

Figure S8. AFM topography map and corresponding CPD maps of Se-free and Se-incorporated films measured under the dark and monochromatic laser illuminations.

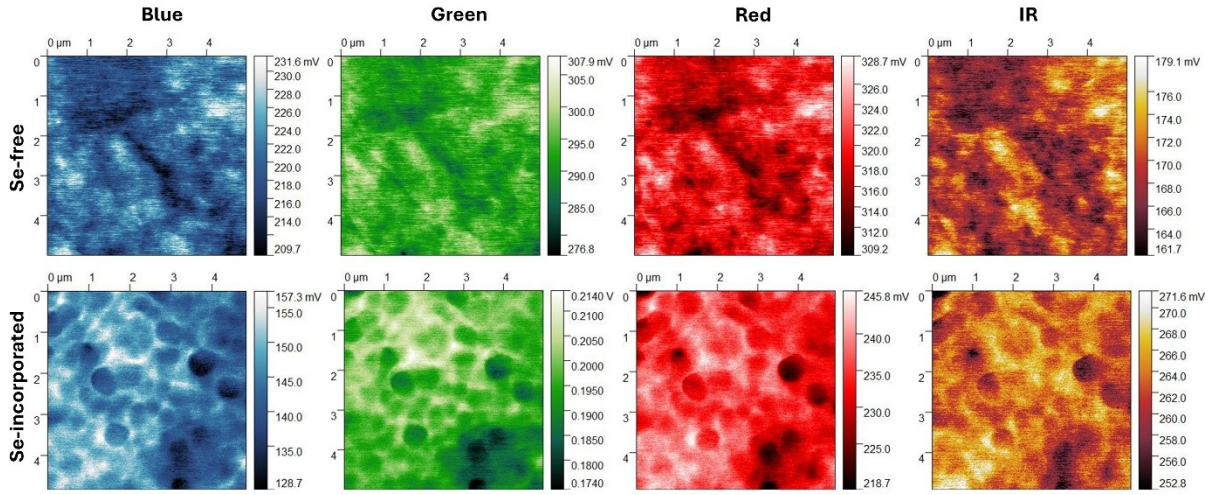

Figure S9. Surface photovoltage (SPV) maps of Se-free and Se-incorporated films calculated from the illuminated and dark CPD measurements.

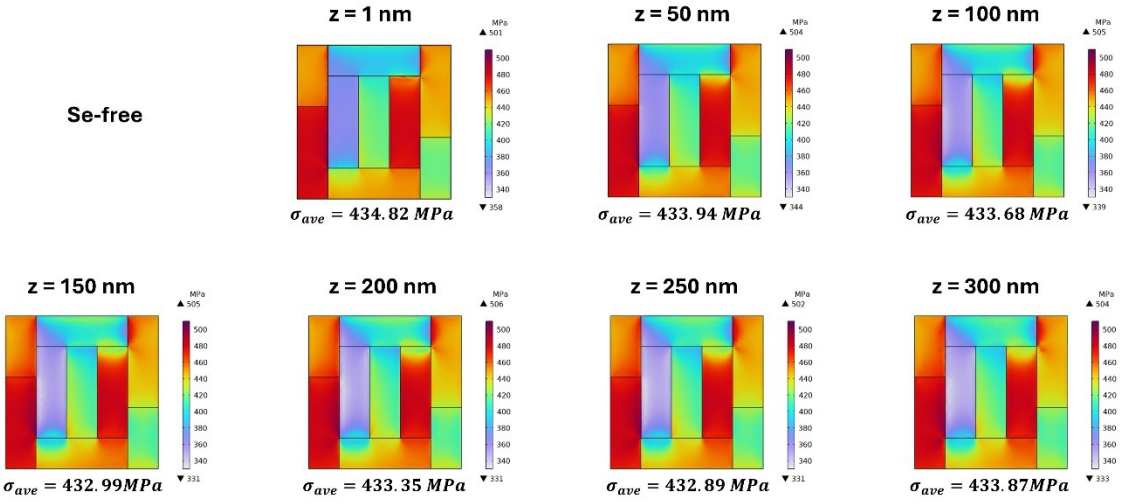

Figure S10. Depth-dependent stress distribution and average von Mises stress (MPa) in the 5 µm × 5 µm × 0.3 µm Se-free film at various depths (z = 1 nm, 50 nm, 100 nm, 150 nm, 200 nm, 250 nm, and 300 nm), simulated using the finite element method (FEM) in COMSOL Multiphysics.

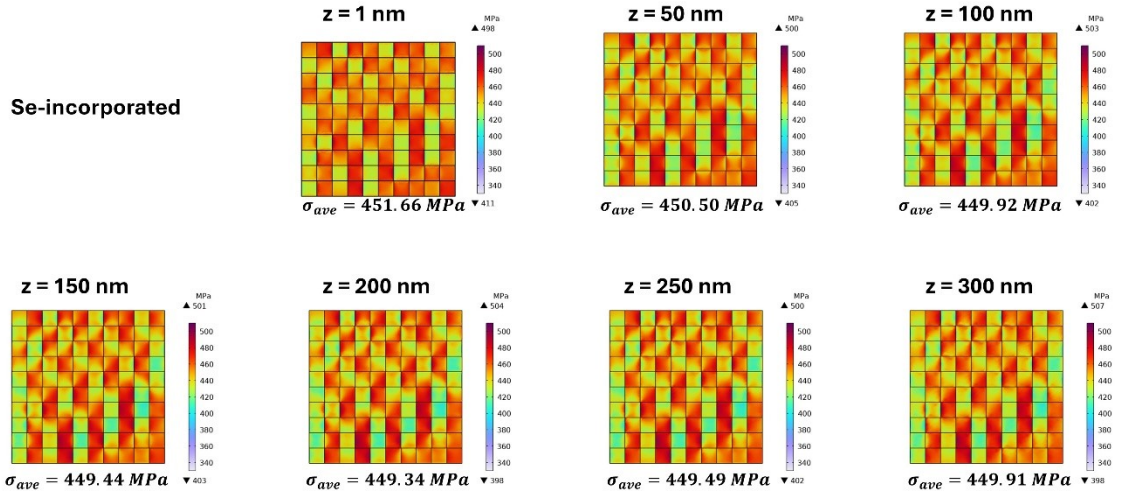

Figure S11. Depth-dependent stress distribution and average von Mises stress (MPa) in the 5 µm × 5 µm × 0.3 µm Se-incorporated film at various depths (z = 1 nm, 50 nm, 100 nm, 150 nm, 200 nm, 250 nm, and 300 nm), simulated using the FEM in COMSOL Multiphysics.

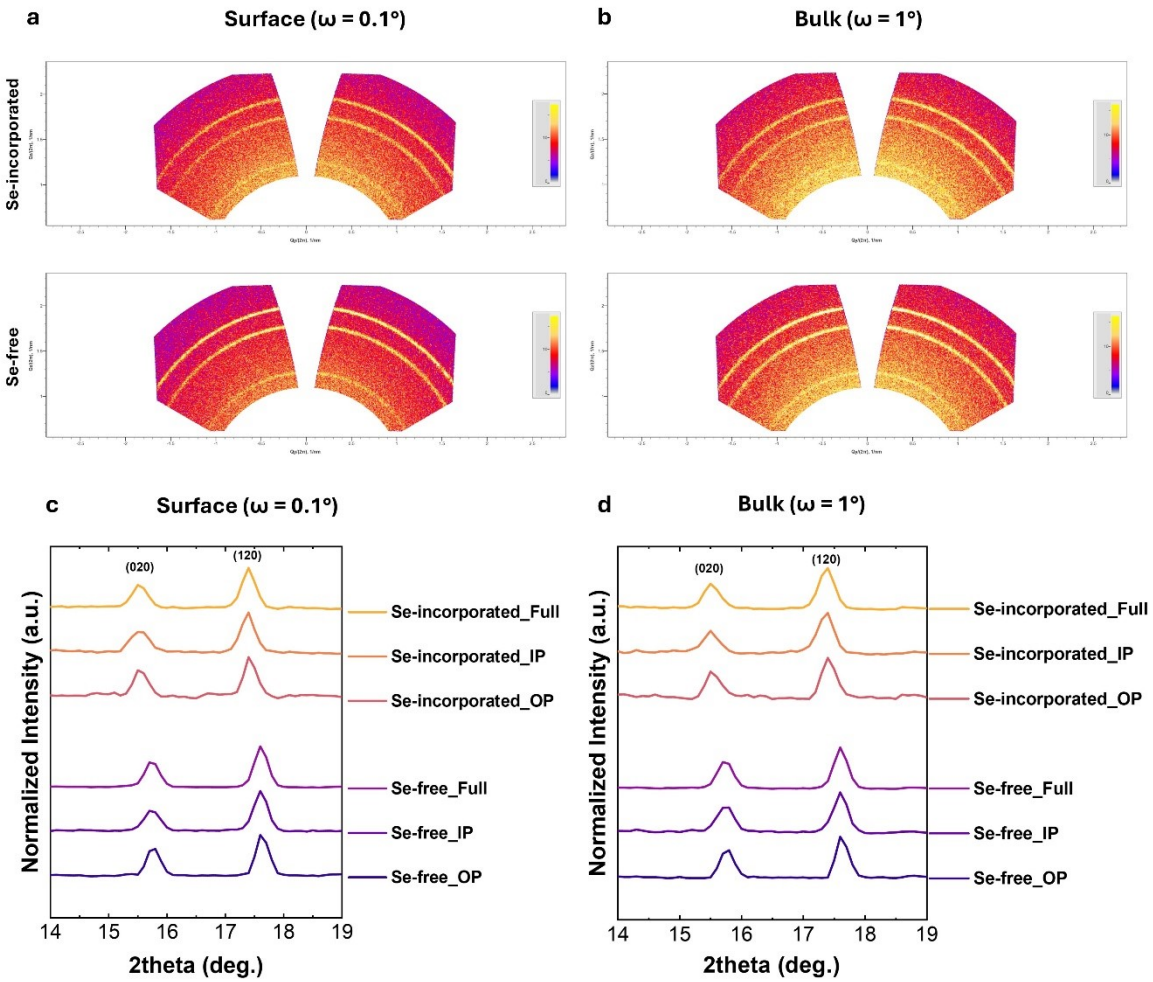

Figure S12. Grazing-incidence wide-angle X-ray scattering (GIWAXS) patterns of Se-free and Se-incorporated films measured at incident angles of (a) 0.1° and (b) 1°, corresponding to surface-sensitive and bulk-sensitive probing depths, respectively. (c, d) In-plane (IP) and out-of-plane (OP) line profiles extracted from the GIWAXS patterns.

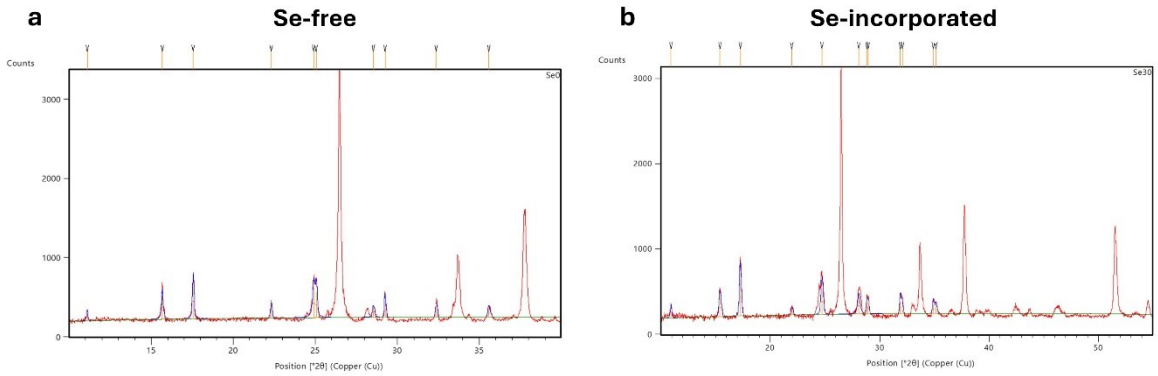

Figure S13. X-ray diffraction (XRD) peak fitting results for (a) Se-free and (b) Se-incorporated films. The detailed peak fitting results are summarized in **Table S3** and **Table S4**.

Table S3. Peak parameters for the Se-free film, including peak position, peak height, FWHM, d-spacing, and relative intensity.

Pos. [°2θ]	Height [cts]	FWHM Left [°2θ]	d-spacing [Å]	Rel. Int. [%]
11.0868	96.91	0.0988	7.97411	22.40
15.6628	291.20	0.0992	5.65321	67.30
17.5490	432.70	0.1076	5.04961	100.00
22.3118	176.08	0.0887	3.98131	40.69
24.8977	365.60	0.1595	3.57334	84.49
25.0584	316.87	0.0946	3.55079	73.23
28.5342	122.12	0.1270	3.12567	28.22
29.2475	165.05	0.0855	3.05104	38.14
32.3753	169.13	0.0974	2.76307	39.09
35.5772	94.16	0.1512	2.52139	21.76

Table S4. Peak parameters for the Se-incorporated film, including peak position, peak height, FWHM, d-spacing, and relative intensity.

Pos. [°2θ]	Height [cts]	FWHM Left [°2θ]	d-spacing [Å]	Rel. Int. [%]
10.9170	72.81	0.0814	8.09781	16.65
15.4090	209.53	0.2501	5.74574	47.93
17.2639	437.21	0.2190	5.13236	100.00
21.9791	62.09	0.2269	4.04080	14.20
24.7256	305.39	0.2415	3.59783	69.85
28.0820	194.74	0.2397	3.17497	44.54
28.8257	139.88	0.1190	3.09472	31.99
28.9677	132.50	0.1151	3.07988	30.31
31.9058	140.09	0.1867	2.80264	32.04
32.0841	59.07	0.0991	2.78747	13.51
34.9025	100.62	0.1950	2.56857	23.01
35.1604	79.46	0.1341	2.55031	18.17

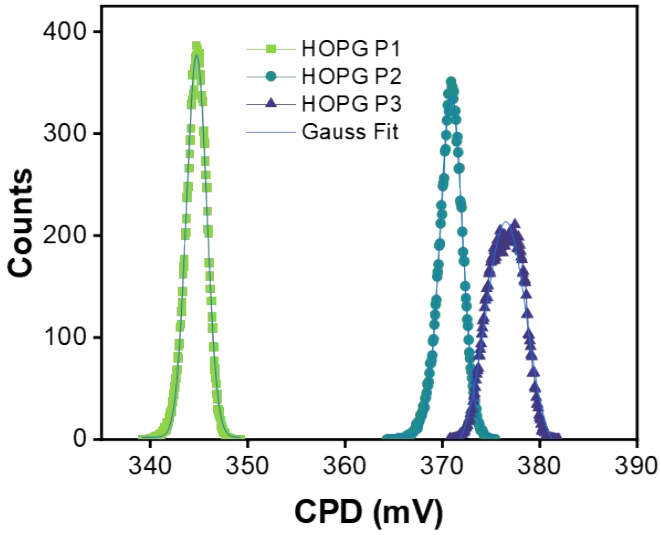

Figure S14. CPD histograms of HOPG with Gaussian fitting for work function calibration of the HQ:DPER-XSC11 Pt-coated AFM tip. P1–P3 denote different spatial points selected for analysis.

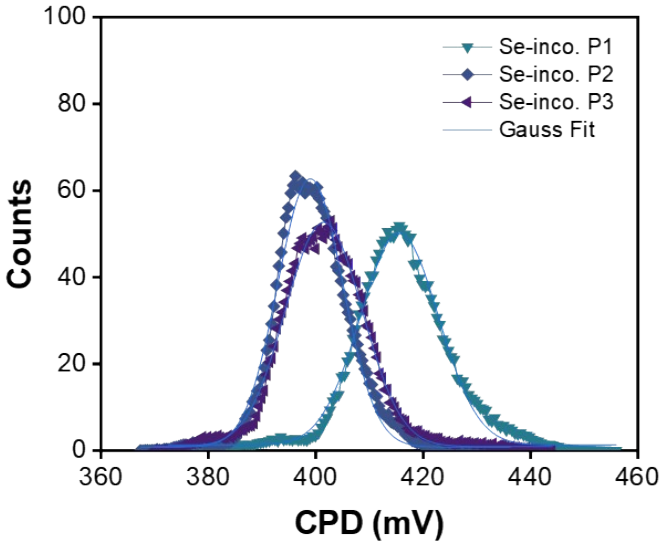

Figure S15. CPD histograms of the Se-incorporated film with Gaussian fitting to extract statistical work function values, measured using the HQ:DPER-XSC11 Pt-coated AFM tip. P1–P3 denote different spatial points selected for analysis.

Table S5. Average CPD values with standard deviations obtained from the CPD measurements shown in Figures S14 and S15.

	CPD (mV)
HOPG P1	344.76
HOPG P2	370.9
HOPG P3	376.52
Average	**364.06**
Standard Deviation	16.95
Se-inco. P1	415.57
Se-inco. P2	398.99
Se-inco. P3	401.49
Average	**405.35**
Standard Deviation	8.94

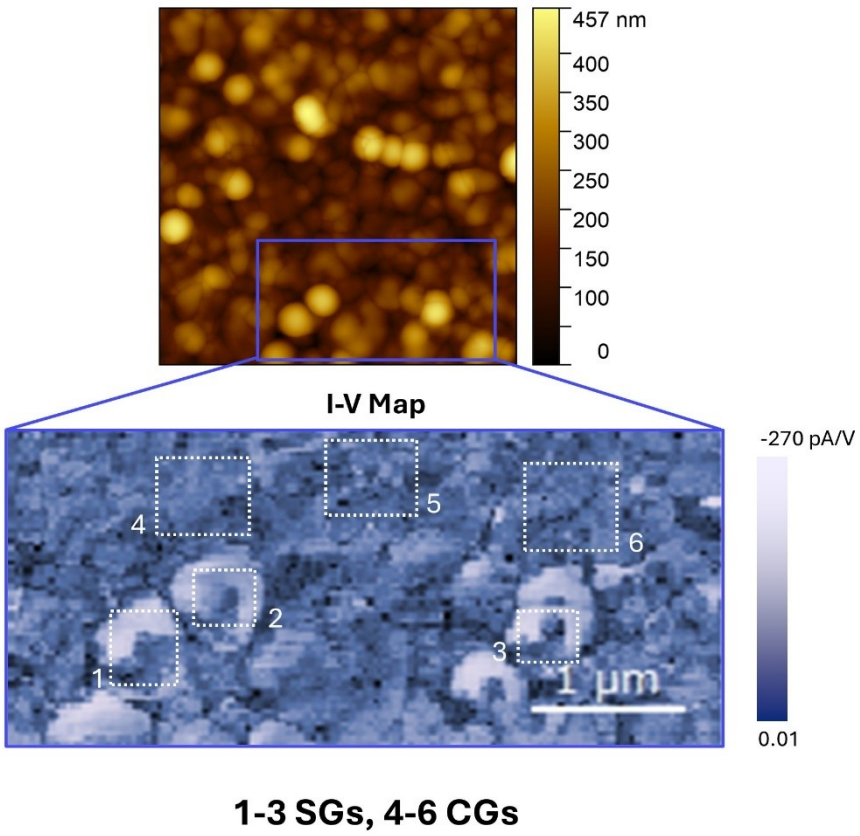

Figure S16. AFM topography image of the Se-incorporated film and regions selected for current–voltage (I–V) analysis using conductive AFM (c-AFM). White boxes indicate the spherical-shaped grain (SG) (1-3) and coalesced grain (CGs) (4-6) areas from which average I–V curves were extracted.

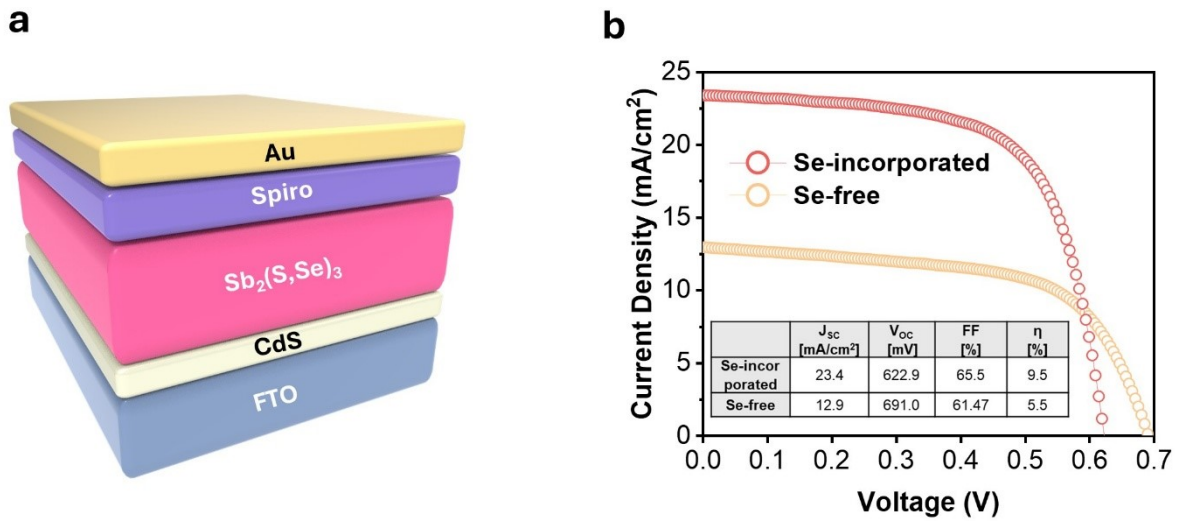

Figure S17. (a) Device structure used for PV measurements. (b) Current density–voltage (J–V) characteristics of the Se-free and Se-incorporated devices. The inset table summarizes the extracted PV parameters: Short-circuit current density (J_{SC}), Open-circuit voltage (V_{OC}), fill factor (FF), and power conversion efficiency (PCE).

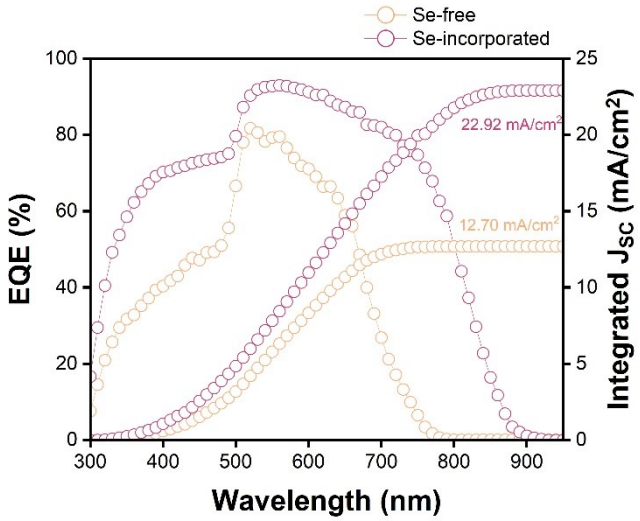

Figure S18. External quantum efficiency (EQE) and integrated J_{SC} spectra of the Se-free and Se-incorporated devices.

Table S6. Materials properties used in FEM simulations for thermal stress analysis [S1–3]

Sample	Density (kg/m^3)	Young's modulus (GPa)	Poisson's ratio	General CTE (10^{-6} K^{-1})	(120) CTE (10^{-6} K^{-1})	(221) CTE (10^{-6} K^{-1})	(020) CTE (10^{-6} K^{-1})	(130) CTE (10^{-6} K^{-1})
Se-free	4980	118.2	0.25	$\alpha_a = 1.86$ $\alpha_b = 13$ $\alpha_c = 6.5$	$\alpha_a = 2.97$ $\alpha_b = 11.89$ $\alpha_c = 6.5$	$\alpha_a = 7.43$ $\alpha_b = 7.33$ $\alpha_c = 6.6$	$\alpha_a = 1.86$ $\alpha_b = 13$ $\alpha_c = 6.5$	$\alpha_a = 4.08$ $\alpha_b = 10.77$ $\alpha_c = 6.5$
Se-incorporated	5355	114.1	0.25	$\alpha_a = 4.7$ $\alpha_b = 12.7$ $\alpha_c = 8.6$	$\alpha_a = 5.5$ $\alpha_b = 11.9$ $\alpha_c = 8.6$	$\alpha_a = 8.7$ $\alpha_b = 8.69$ $\alpha_c = 8.61$	$\alpha_a = 4.7$ $\alpha_b = 12.7$ $\alpha_c = 8.6$	$\alpha_a = 6.3$ $\alpha_b = 11.1$ $\alpha_c = 8.6$

Reference

S1 H. Koc, A. M. Mamedov, E. Deligoz and H. Ozisik, *Solid State Sci.,* 2012, **14**, 1211–1220.

S2 M. G. Herrmann, R. P. Stoffel, I. Sergueev, H.-C. Wille, O. Leupold, M. Ait Haddouch, G. Sala, D. L. Abernathy, J. Voigt, R. P. Hermann, R. Dronskowski and K. Friese, *Phys. Status Solidi B,* 2020, **257**, 2000063.

S3 C. K. Gan, J. R. Soh and Y. Liu, *Phys. Rev. B,* 2015, **92**, 235202.